JTTEE5 15:184-190
DOI: 10.136/105996306X107995
1059-9630/$19.00 © ASM International

Peer Reviewed

Cold-Spray Processing of a Nanocrystalline Al-Cu-Mg-Fe-Ni Alloy with Sc

L. Ajdelsztajn, A. Zúñiga, B. Jodoin, and E.J. Lavernia

(Submitted August 26, 2005; in revised form November 3, 2005)

This work describes recent progress in cold-spray processing of conventional and nanocrystalline 2618 (Al-Cu-Mg-Fe-Ni) aluminum alloy containing scandium (Sc). As-atomized and cryomilled 2618 + Sc aluminum powder were sprayed onto aluminum substrates. The mechanical behavior of the powders and the coatings were studied using micro- and nanoindentation techniques, and the microstructure was analyzed using scanning and transmission electron microscopy (SEM and TEM). The influence of powder microstructure, morphology, and behavior during deposition on the coating properties was analyzed. This work shows that Al-Cu-Mg-Fe-Ni-Sc coatings with a nanocrystalline grain structure can be successfully produced by the cold-spray process. Inspection of the scientific literature suggests that this is the first time a hardness value of 181 HV has been reported for this specific alloy.

Keywords cold gas dynamic spraying, nanostructured coatings, nanostructured materials

1. Introduction

A new spraying technology called the cold gas dynamics spraying process (CGDS), first developed in the mid-1980s at the Institute of Theoretical and Applied Mechanics in Russia (Ref 1), was introduced at the laboratory scale in North America in the 1990s (Ref 2-5). Derived from other thermal spray processes, it uses a supersonic gas jet to accelerate solid fine powders (micron size) of various materials above a critical velocity at which particles impact, deform plastically, and bond to the substrate to form a coating. As cold spray is a new and emerging spray process, many aspects of this process, both experimental and theoretical, have been explored in recent years.

Because the particle adheres to the substrate following a solid-state plastic deformation process, cold spray is referred to as a solid-state process. The main advantage of such a deformation mode, as opposed to plasma or high-velocity oxygen-fuel (HVOF) spraying, is the possibility of retaining the microstructural, mechanical, and chemical properties of the particle feedstock. Numerous types of materials have been successfully sprayed; most frequently, copper (Ref 3, 6-8), aluminum (Ref 1, 8-10), titanium (Ref 2), and nickel and nickel alloys (Ref 3). Recently, nanocrystalline aluminum alloys were also sprayed using the cold-spray process (Ref 11).

The original version of this paper was published in the CD ROM *Thermal Spray Connects: Explore Its Surfacing Potential*, International Thermal Spray Conference, sponsored by DVS, ASM International, and IIW International Institute of Welding, Basel, Switzerland, May 2-4, 2005, DVS-Verlag GmbH, Düsseldorf, Germany.

L. Ajdelsztajn, A. Zúñiga, and **E.J. Lavernia,** Department of Chemical Engineering and Materials Science, University of California, Davis, CA 95616; and **B. Jodoin,** Department of Mechanical Engineering, University of Ottawa, Ontario, Canada K1N 6N5. Contact e-mail: lajd@ucdavis.edu.

Al-Cu alloys have been used extensively in the past in aerospace, aeronautics, and automotive applications due to their high strength up to intermediate temperatures (~200 °C) (Ref 12). The normal aging sequence after a high temperature solution treatment is as follows (Ref 13): supersaturated solid solution → Guinier-Preston (GP) zones → θ″ → θ′ → θ, where the metastable phases θ″ and θ′ are responsible for the high strength observed in this type of alloy (Ref 14). The addition of alloying elements in Al-Cu alloys (such as Mg or Ag) has also been investigated, resulting in the formation of novel metastable intermetallic phases (such as Ω Al_2Cu) (Ref 15). In the case of low Cu, high Mg alloys, the main strengthening phase changes from platelike θ′ (metastable form of Al_2Cu) to rod-shaped S′ (metastable form of Al_2CuMg) (Ref 16), giving rise to a more stable system. Further development of alloys with a low Cu/Mg ratio gave rise to the 2618 aluminum alloy (Al-Cu-Mg-Fe-Ni) for intermediate temperatures (~230 °C), where the addition of Fe and Ni (1 wt.% each) promotes the formation of stable Al_9FeNi intermetallics (Ref 17). The most famous application of the 2618 alloy is in the fuselage of the former supersonic civil transportation vehicle, the Concorde (Ref 18).

Similarly, Al-Sc alloys have also engendered considerable interest as a result of their superior strength (Ref 19). The main source of strengthening in this type of alloy is derived from the precipitation of a uniform distribution of nanosized Al_3Sc particles (Ref 20). These particles are resistant to coarsening, remain coherent up to 30 nm (Ref 21), and have the highest specific strengthening effect in Al (in an atom-to-atom basis) (Ref 22). Our research group is currently investigating the effect of adding Sc to Al-Cu-Mg-Fe-Ni alloys; however, the main purpose of this paper is to study how a nanocrystalline grain structure in the Al-Cu-Mg-Fe-Ni-Sc alloy affects the coating formation during cold spray, rather than the effect of Sc on the properties of such a coating.

The microstructure and mechanical behavior of solid-solution strengthened, nanocrystalline Al alloys have been extensively studied by the authors' research group (Ref 23, 24). The most important characteristics of these nanocrystalline Al alloys are their high strength and high thermal stability. The pro-

Table 1 Chemical composition of the powder, wt.%

Cu	Mg	Fe	Ni	Si	Sc	Al
2.3	1.47	1.08	1.0	0.19	0.16	Bal

Table 2 N, O, and H content in the as-cryomilled powder

N, wt.%	O, wt.%	H, ppm
0.723	0.711	420

cessing technique used to produce these nanocrystalline structures is cryomilling, which consists of mechanical milling under a liquid nitrogen atmosphere. Nanocrystalline, heat-treatable Al-Cu alloys (such as Al-Cu-Mg-Fe-Ni-Sc) produced by cryomilling have not yet been investigated.

The main objectives of the current study are to investigate and compare the microstructure and properties of conventional and nanocrystalline Al-Cu-Mg-Fe-Ni-Sc coatings produced using the cold gas dynamic spraying technology.

2. Experimental Procedure

2.1 Powder Preparation

The Al-Cu-Mg-Fe-Ni-Sc powder was produced by gas atomization using nitrogen as the inert atmosphere as well as the atomizing gas. The atomization temperature and dynamic pressure were 840 °C and 200 psi, respectively. The chemical composition of the as-atomized powder is presented in Table 1.

The as-atomized powder was also mechanically milled at the rate of 180 rpm in a modified Union Process 01-ST (Akron, OH) attritor for 8 h under a liquid nitrogen environment, which was continuously supplied during milling to ensure complete immersion of the powders. Stainless steel balls 6.4 mm in diameter were used as the grinding media, and a ball-to-powder weight ratio of 32:1 was selected. Details of the cryomilling system are described elsewhere (Ref 25). The impurity content in the as-cryomilled powder is shown in Table 2. Finally, after atomization and cryomilling, the powders were sieved to less than 25 μm using a 500 mesh (Ref 26).

2.2 Coating Preparation

The as-atomized and as-cryomilled powders were sprayed onto grit blasted (20 mesh grit) Al substrates using the cold spray coating system developed at the University of Ottawa; a cold spray facility that has been used extensively to spray a variety of coatings (Ref 23). It consists of a gas control system, a commercial powder feeder (Praxair 1264, Indianapolis, IN, powder feeder), a spray gun, and a sealed off spraying chamber, providing the possibility of recycling the powder that has not adhered to the substrate. The gun is a converging-diverging nozzle allowing the particles to reach the high velocities required in the process (~700 m/s). The nozzle exit diameter is 6.3 mm. The system incorporates two probes that measure the temperature and pressure before the converging section. The substrate holder is equipped with a one-axis travel displacement system. Helium gas at room temperature was used as the driving and carrier gas. The stagnation pressure was set at 1.7 MPa, while the injection pressure was set to provide a pressure difference of 35 kPa at the injection site. One pass was performed to build-up the coating on the substrate, and a spray distance of 20 mm was used.

2.3 Powder and Coating Characterization

The morphology of the powders and the microstructure of the coatings were examined using a Philips XL30 (Hillsboro, OR) FEG SEM. Prior to scanning electron microscopy (SEM) observations, the coating samples were sectioned from a transverse section and prepared by standard metallographic techniques. Secondary electron and backscattered electron images were obtained, and energy dispersive spectrometry (EDS) analyses were conducted on the coating samples.

The microstructure of the coatings was also analyzed by transmission electron microscopy (TEM) using a Philips CM 12 (Hillsboro, OR) microscope operated at 100 kV. The samples were prepared by jet polishing using a mixture of 70% methanol and 30% nitric acid kept at −30 °C.

To investigate the mechanical properties of the powders and coatings, nanoindentation studies were conducted in a MTS Nanoindenter XP (Berkovich, Oak Ridge, TN, indenter) on the cross section of the powders and the sprayed coatings. Powder samples were prepared for nanoindentation by mixing the cryomilled powder with a conductive molding compound. The samples were then ground (1200 grit) and polished (6, 3, 1, 0.25 μm diamond slurry). The same polishing procedures were used to prepare the cross section of the sprayed coatings. The continuous stiffness measurement (CSM) approach was used to determine the hardness values from the nanoindentation tests (Ref 27). An indentation depth of 500 nm was chosen in this study. Vickers microhardness tests were also performed on the cross section of the coatings using 300 gf of load and a dwell time of 15 s in a Buehler Micromet 2004 (Lake Bluff, IL) indenter. The reported values are the average of 15 indentations for each sample.

3. Results and Discussion

3.1 Powder Characterization

The morphology of the atomized and cryomilled powders is shown in Fig. 1. The morphology of the atomized powder is spherical, in agreement with what is usually seen in gas-atomized powder (Fig. 1a); on the other hand, mechanical cryomilling of the gas atomized spherical powder led to the formation of irregular and flake-shaped agglomerates, as shown in Fig. 1(b). This morphology is attributed to the continuous welding and fracturing of the powder particles during the mechanical milling process (Ref 25).

The microstructure of the as-cryomilled powder is shown in the bright field TEM image of Fig. 2. It mainly consists of equiaxed, nanometric aluminum grains of approximately 50 nm, along with some slightly larger elongated grains. The presence of small Al_9FeNi particles that were broken down during the cryomilling process was also detected.

The development of nanostructures during cryomilling can be described as a three-stage process of grain refinement (Ref 25). The first stage is the localization of deformation into shear bands with high dislocation density, which is followed by anni-

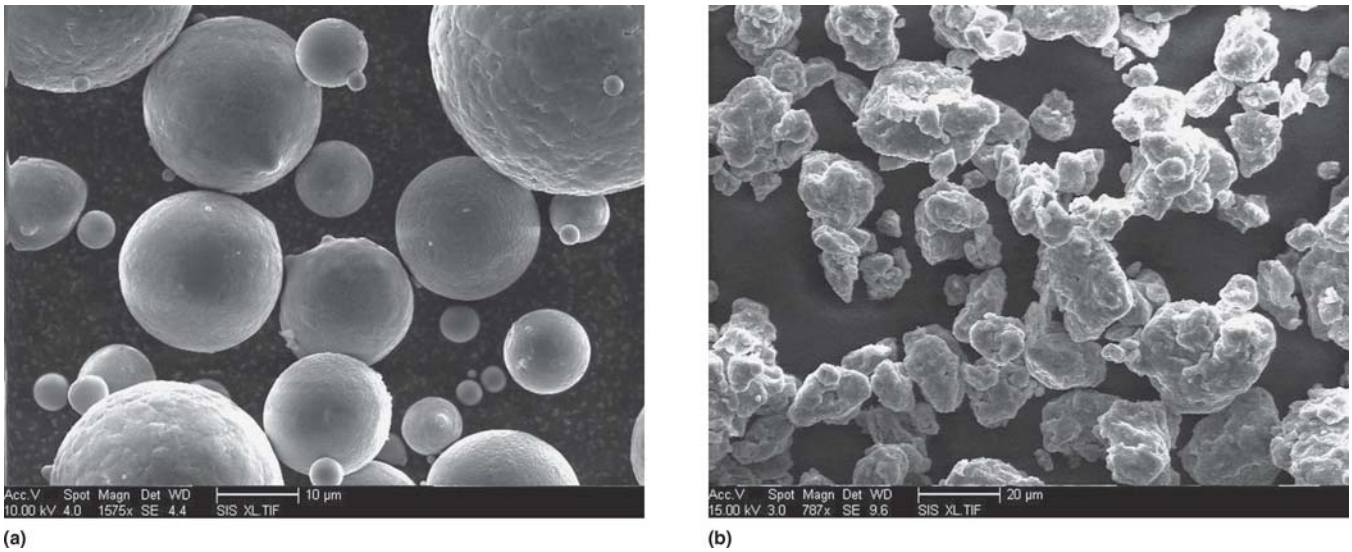

Fig. 1 Morphology of the powder: (a) as-sprayed and (b) as-cryomilled

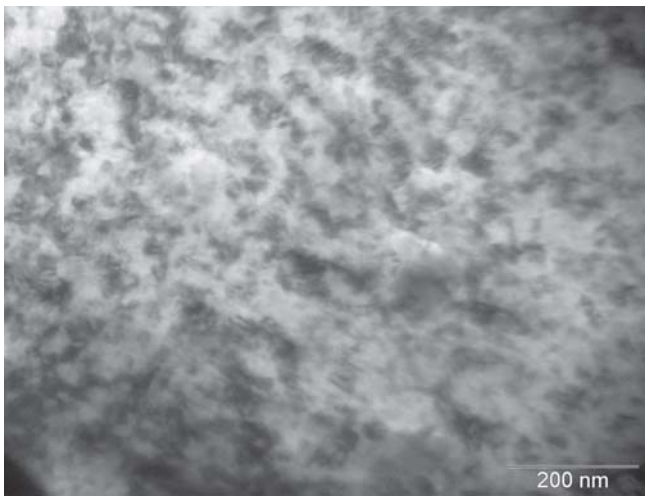

Fig. 2 TEM micrograph showing the microstructure of the as-cryomilled powder

hilation and recombination of dislocations, forming nanometer-scale subgrains. This subgrain structure extends throughout the sample during continued milling. The final stage is the transformation of subgrain boundary structure to randomly oriented high-angle grain boundaries forming the nanocrystalline grains observed in Fig. 2.

3.2 Coating Microstructure

Figures 3(a) and (b) show secondary and backscattered electron images of the coatings produced from the gas-atomized powders, whereas Fig. 3(c) and (d) show the same for the coatings produced from the cryomilled powders. Figure 3(a) demonstrates that limited or no porosity is present in the coating. Furthermore, the interface between the coating and the substrate can barely be detected in secondary electron mode. Only in the backscattered electrons mode (Fig. 3b) can the interface between the substrate and the coating be revealed. Also, the presence of intermetallics at the grain boundary of the alloy (shown in the backscattered image) facilitates the investigation of the deformation that the powders were subjected to during impact. These intermetallics correspond to Al_2CuMg located at the grain boundaries and Al_9FeNi precipitates distributed throughout the matrix (detail shown in Fig. 4a). The same microstructure is observed in the atomized powder and it is described in detail elsewhere (Ref 28).

The situation is different in the nanocrystalline coating, in which the porosity (between 5 and 10%) is substantially higher than in the conventional coating (Fig. 3c). In the nanocrystalline coating, not only can the interface between the coating and the substrate be observed, but the particle/particle boundaries are also clearly observed, indicating that the processes that helped produce a dense coating using the conventional powder (such as deformation and shear instability) were less effective in the nanocrystalline case. Moreover, because of its fine microstructure, the nanocrystalline coating (produced from the cryomilled powder) shows no microstructure details in the SEM images besides the dispersed Al_9FeNi submicron particles (Fig. 4b).

The lack of defects and porosity at the particle-particle and particle-substrate interfaces in the conventional coating (Fig. 4a) suggests an adequate kinetic energy during deposition that was able to break off the surface oxide film and generate intimate bonding at the interfaces of the coating. Two different deformation processes occur during impact: one is related to the deformation of the particle upon impact (splat behavior in solid state), and the other is a localized deformation process that is present at the particle boundaries (jet flow or adiabatic shear instability) (Ref 29). The first one is responsible for the mechanical locking of the constituent particles in the coating, and the second one occurs at the boundary of the particles and promotes an intimate metallic bonding between adjacent particles by breaking off the oxide layer that is naturally present in the feedstock aluminum

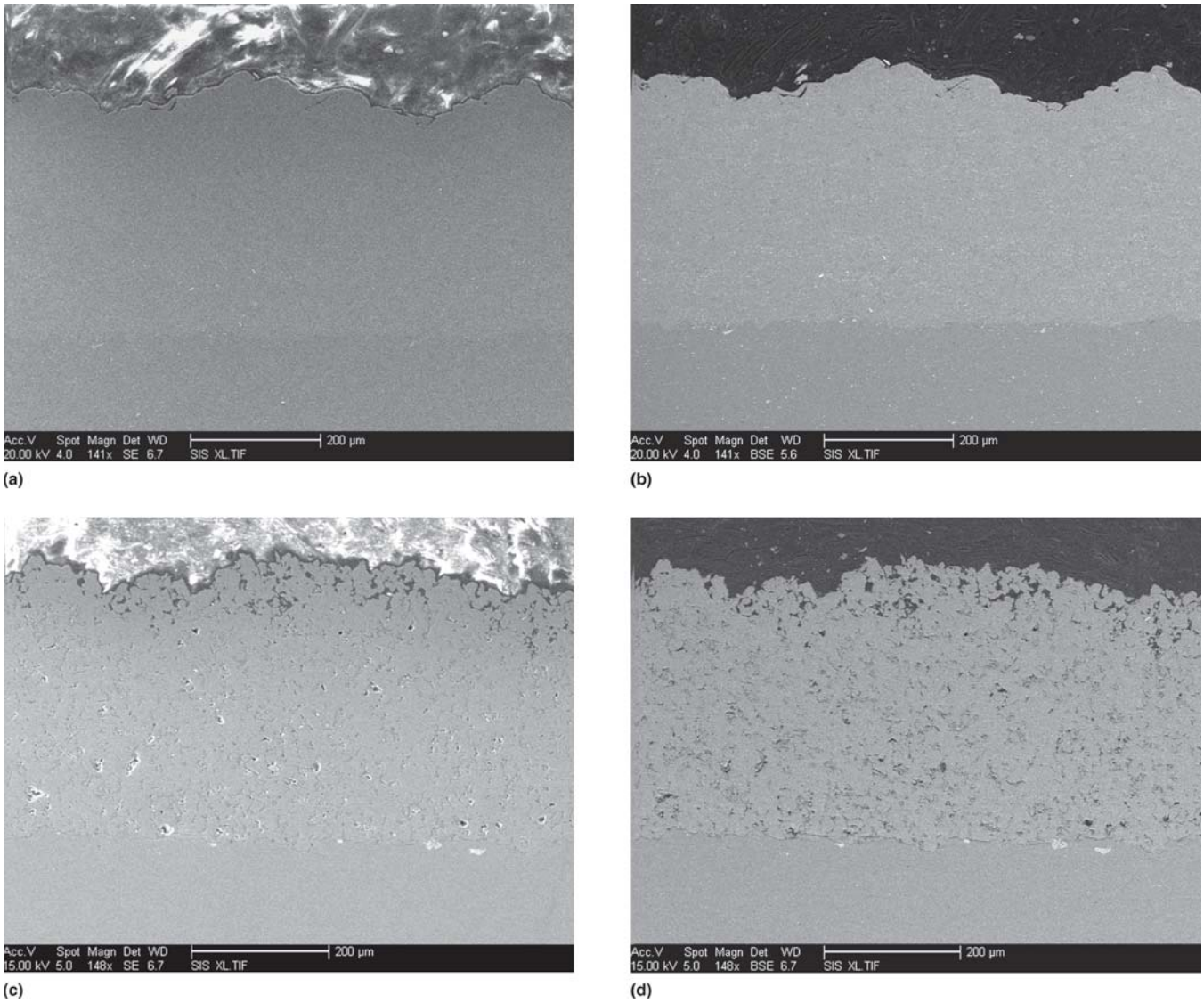

Fig. 3 Cold-sprayed coatings: (a, b) conventional and (c, d) nanocrystalline

powder. The adiabatic regimen during the particle impact can lead to thermal softening that would facilitate the plastic deformation and interlocking of splats, each particle conformably shaping to the previous layer producing a dense coating. The localized adiabatic shear instability at the particles boundaries helps the creation of intimate contact between clean surfaces that result in metallurgical bonding at the particle-particle surfaces. Moreover, the intense shear localization at the particles boundaries addresses a critical point when aluminum alloys are sprayed, which is the disruption of the protective oxide layer. Microstructural evidence of localized shear instabilities in the alloy material used in this work can be found elsewhere (Ref 28).

As shown in Fig. 1(b), the cryomilling process produced nonspherical particles. From the aerodynamics perspective, this is beneficial for the powder acceleration as the drag coefficient of nonspherical particles is larger than the drag coefficient of spherical particles with the same mass (and volume) (Ref 30). As a consequence, a larger drag force will be applied to the nonspherical particles, promoting higher velocity at the end of the acceleration zone of the nozzle. Nevertheless, the cryomilled powder, when sprayed under the same conditions used for the as-atomized powder, did not generate coatings with the same level of densification. This behavior could be attributed to the fact that the cryomilled powder is much harder and difficult to deform, hence promoting the presence of porosity during deposition (Fig. 3c). The TEM image in Fig. 5 shows that the overall microstructure of the coating did not change compared to the as-cryomilled powder, i.e., equiaxed grains of approximately 50 nm in size and nanosized intermetallic particles (mainly Al_9FeNi) dispersed throughout the matrix. Also, there is no microstructural evidence of a heavily deformed grain structure in the nanocrystalline particles upon impact during cold spray, which suggests that the main deformation mechanism may not be dislocation plasticity. However, a more detailed study is needed to clarify this issue.

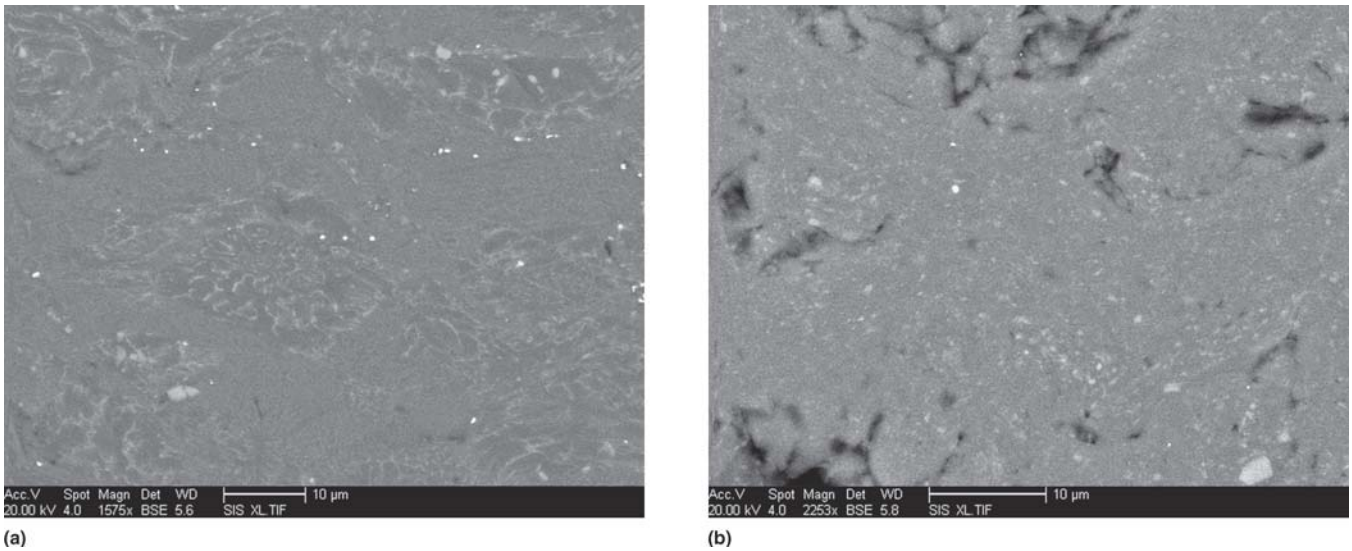

Fig. 4 SEM micrographs showing details in the microstructure of the coatings: (a) conventional and (b) nanocrystalline

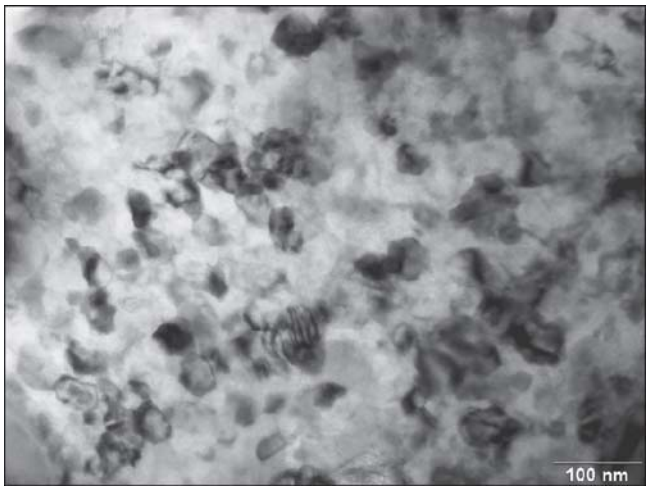

Fig. 5 TEM micrograph of the nanocrystalline coating

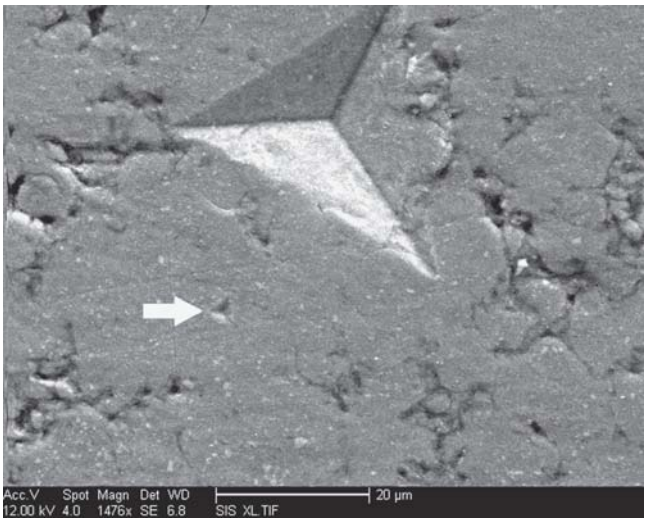

Fig. 6 Nanoindentation marks on the cross section of the nanocrystalline cold-sprayed coating (5 µm and 500 nm indentation depth)

3.3 Mechanical Behavior

Figure 6 shows two indentation marks on the nanocrystalline coating, one 5 µm in depth and the other with a much small penetration depth (500 nm). It can be seen that interlamellar defects such as interlamellar cracks or porosity are not present in the surrounding area of the small indentation mark. Furthermore, it can be argued that when the indentation depth decreases, the hardness measurement is related to the intrinsic properties of the constituent material of the coating (intralamellar properties) and is not affected by microstructural defects such as porosity and cracks. The nanoindentation results (500 nm in depth) for the powders and coatings are presented in Table 3. The hardness of the nanocrystalline powder is substantially higher than that of the conventional one. Similarly, the hardness of the nanocrystalline coating is higher than that of the conventional one. The difference in hardness between the nanocrystalline and conventional microstructures is well documented and can be rationalized on the basis of the Hall-Petch relationship for polycrystalline materials (Ref 31, 32).

Table 3 Nanoindentation data, GPa

As-atomized powder	As-cryomilled powder	Conventional coating	Nanocrystalline coating
2.32 ± 0.2	4.19 ± 0.2	3.75 ± 0.3	4.41 ± 0.5

It can be observed that the hardness of the conventional coating is higher than that of the conventional powder, which suggests that the powder exhibited work hardening upon impact, increasing the density of dislocations within the grains and, therefore, the hardness of the coating. On the contrary, the hardness of the nanocrystalline coating is similar to that of the as-cryomilled powder, suggesting, as described before, that there is

no microstructural evidence of a heavily deformed grain structure in the cryomilled powder upon impact that can promote an increase in hardness (limited or no work hardening is observed).

The nanocrystalline coating has a much higher hardness than the conventional one, which can be also attributed to the small grain size. This is a good indication that no or minimal melting occurred during spraying, showing that the initial nanostructure of the powder is retained in the coating after the cold spray process. Therefore, the cold spray process, along with the cryomilling technique, can be successfully applied to produce nanocrystalline coatings.

Finally, it is worth mentioning that the Vickers hardness of the conventional coating is similar to that of solution treated and peak aged commercial 2618 (145 HV; Ref 24). On the other hand, the high hardness value of 181 HV (300 g) observed in the nanocrystalline coating has never been previously reported for this type of Al-Cu-Mg-Fe-Ni-Sc alloy, and is considerably higher than both the conventional coating and bulk peak aged 2618 alloy.

4. Conclusions

Cold-spray deposition of conventional and nanocrystalline Al-Cu-Mg-Fe-Ni-Sc coatings was successfully achieved. The conventional cold-sprayed coating showed negligible porosity and an excellent interface with the substrate material. This was not the case for the nanocrystalline coating, in which the porosity level was in the range of 5-10%. The microstructure of the feedstock powders (atomized and cryomilled) was retained after the cold-spray process.

The difference in porosity between the conventional and nanocrystalline coatings can be explained by the hardness and microstructure of the corresponding feedstock powder: the softer and coarse-grain conventional powder experienced generalized adiabatic shear instability upon impact, resulting in a dense coating, whereas the harder and fine-grain cryomilled powder did not exhibit the same extent of deformation, resulting in a less dense coating.

Similarly, the conventional powder showed work hardening during impact, thus increasing the hardness of the conventional coating compared with the feedstock powder. On the other hand, the hardness of the nanocrystalline coating was similar to that of the feedstock powder, suggesting that no work hardening took place in this case.

The Vickers microhardness of the nanocrystalline coating was, despite the porosity, much higher than that of the conventional coating, showing that a nanocrystalline structure has a strong effect on the overall mechanical behavior of the coating. Finally, to the best of the authors' knowledge, this is the first time that a hardness value of 181 HV has been reported for this specific alloy.

Acknowledgment

The authors gratefully acknowledge the financial support given by the Office of Naval Research under Contract No. N00014-04-1-0370.

References

1. A.P. Alkhimov, V.F. Kosarev, and A.N. Papyrin, Gas Dynamic Method for Applying Coating, U.S. Patent 5,302,414, December 4, 1994
2. C.J. Li and W.Y. Li, Deposition Characteristics of Titanium Coating in Cold Spraying, *Surf. Coat. Technol.,* 2003, **167**(2-3), p 278-283
3. A.P. Alkhimov, S.V. Klinkov, V.F. Kosarev, and A.N. Papyrin, Gas-dynamic Spraying. Study of a Plane Supersonic Two-phase Jet, *J. Appl. Mech. Tech. Phys.,* 1997, **38**(2), p 324-330
4. R.C. Dykhuizen and R.A. Neiser, Optimizing the Cold Spray Process, *Thermal Spray 2003: Advancing the Science and Applying the Technology*, B.R. Marple and C. Moreau, Ed., May 5-8, 2003 (Orlando, FL), ASM International, 2003, p 19-26
5. A.N. Papyrin, V.F. Kosarev, S.V. Klinkov, and A.P. Alkhimov, On the Interaction of High Speed Particles with a Substrate under Cold Spraying, *International Thermal Spray Conference*, E. Lugscheider and C.C. Berndt, Ed., March 4-6, 2002 (Essen, Germany), DVS Deutscher Verband für Schweißen, 2002, p 380-384
6. R.C. Dykhuizen, M.F. Smith, D.L. Gilmorew, and R.A. Neiser, Impact of High Velocity Cold Spray Particles, *J. Therm. Spray Technol.,* 1999, **8**(4), p 559-564
7. D.L. Gilmore, R.C. Dykhuizen, R.A. Neiser, T.J. Roemer, and M.F. Smith, Particle Velocity and Deposition Efficiency in the Cold Spray Process, *J. Therm. Spray Technol.,* 1999, **8**(4), p 576-582
8. T.H. Van Steenkiste, J.R. Smith, and R.E. Teetse, Aluminum Coatings via Kinetic Spray with Relatively Large Powder Particles, *Surf. Coat. Technol.,* 2002, **154**(2-3), p 237-252
9. H. Assadi, F. Gartner, T. Stoltenhoff, and H. Kreye, Bonding Mechanism in Cold Gas Spraying, *Acta Mater.,* 2003, **51**(15), p 4379-4394
10. J. Vlcek, H. Huber, H. Voggenreiter, A. Fischer, E. Lugscheider, and H. Hallen, Kinetic Powder Compaction Applying the Cold Spray Process: A Study on Parameters, *Thermal Spray 2001: New Surfaces for a New Millennium*, C.C. Berndt, K.A. Khor, and E.F. Lugscheider, Ed., May 28-30, 2001 (Singapore), ASM International, 2001, p 417-422
11. L. Ajdelsztajn, B. Jodoin, G.E. Kim, and J.M. Schoenung, Cold Spray Deposition of Nanocrystalline Aluminum Alloys, *Metall. Mater. Trans. A,* 2005, **36A**(3), p 657-666
12. I.J. Polmear, Recent Developments in Light Alloys, *Mater. Trans, JIM,* 1996, **37**(1), p 12-31
13. V. Gerold, On the Structures of Guinier-Preston Zones in Al-Cu alloys, *Scripta Metall.,* 1988, **22**(7), p 927-932
14. P.G. Shewmon, *Transformation in Metals,* McGraw-Hill, New York, 1969.
15. I.J. Polmear and M.J. Couper, Design and Development of an Experimental Wrought Aluminum-alloy for Use at Elevated-Temperatures, *Metall. Trans. A,* 1988, **19A**(4), p 1027-1035
16. A. Roósz and H.E. Exner, Ternary Restricted-Equilibrium Phase-Diagrams 2. Practical Application—Aluminum-Rich Corner of the Al-Cu-Mg System, *Acta Metall. Mater.,* 1990, **38**(10), p 2009-2016
17. I.N.A. Oguocha and S. Yannacopoulos, Precipitation and Dissolution Kinetics in Al-Cu-Mg-Fe-Ni Alloy 2618 and Al-Alumina Particle Metal Matrix Composite, *Mater. Sci. Eng. A,* 1997, **231**(1-2), p 25-33
18. J. Majimel, G. Molénat, M.J. Casanove, D. Schuster, A. Denquin, and G. Lapasset, Investigation of the Evolution of Hardening Precipitates During Thermal Exposure or Creep of a 2650 Aluminium Alloy, *Scripta Mater.,* 2002, **46**(2), p 113-119
19. L.S. Toropova, D.G. Eskin, M.L. Kharakterova, and T.V. Dobatkina, *Advanced Aluminum Alloys Containing Scandium,* Gordon and Breach, Amsterdam, The Netherlands, 1998.
20. D.N. Seidman, E.A. Marquis, and D.C. Dunand, Precipitation Strengthening at Ambient and Elevated Temperatures of Heat-treatable Al(Sc) Alloys, *Acta Mater.,* 2002, **50**(16), p 4021-4035
21. G.M. Novotny and A.J. Ardell, Precipitation of Al_3Sc in Binary Al–Sc Alloys, *Mater. Sci. Eng. A,* 2001, **318**(1-2), p 144-154
22. E.A. Marquis and D.N. Seidman, Nanoscale Structural Evolution of Al_3Sc Precipitates in Al(Sc) Alloys, *Acta Mater.,* 2001, **49**(11), p 1909-1919
23. B.Q. Han and E.J. Lavernia, Deformation Mechanisms of Nanostructured Al Alloys, *Adv. Eng. Mater.,* 2005, **7**(6), p 457-465
24. B.Q. Han, D. Matejczyk, F. Zhou, Z. Zhang, C. Bampton, E.J. Lavernia, and F.A. Mohamed, Mechanical Behavior of a Cryomilled Nanostruc-

tured Al-7.5 pct Mg Alloy, *Metall. Mater. Trans. A,* 2004, **35A**(3), p 947-949
25. D.B. Witkin and E.J. Lavernia, Synthesis and Mechanical Behavior of Nanostructured Materials via Cryomilling, *Prog. Mater. Sci.,* 2006, **51,** p 1–60
26. "Standard Specification for Wire Cloth and Sieves for Testing Purposes," E-11, *Annual Book of ASTM Standard,* ASTM, Vol. 14.02
27. X. Li and B. Bhushan, A Review of Nanoindentation Continuous Stiffness Measurement Technique and its Applications, *Mater. Characterization,* 2002, **48**(1), p 11-36
28. L. Ajdelsztajn, A. Zúñiga, B. Jodoin, and E.J. Lavernia, Cold Gas Dynamic Spraying of a High Temperature Al Alloy, *Surf. Coat. Technol.,* 2005, (in press)
29. T.W. Wright, Shear Band Susceptibility: Work Hardening Materials, *Int. J. Plast.,* 1992, **8**(2), p 583-602
30. J.J. Bertin, *Hypersonic Aerothermodynamics,* AIAA, Reston, VA, 1994
31. E.O. Hall, The Deformation and Ageing of Mild Steel: III Discussion of Results, *Proc. Phys. Soc.London,* 1951, **B64,** p 747-753
32. N.J. Petch, The Cleavage Strength of Polycrystals, *J. Iron. Steel Inst.,* 1953, **174,** p 25-28